SF2A 2023
M. N'Diaye, A. Siebert, N. Lagarde, O. Venot, K. Baillié, M. Béthermin, E. Lagadec, J. Malzac, J. Richard (eds)

PROBING THE ATTENUATION CURVE OF $1 < Z < 3$ GALAXIES WITH THE JWST/CEERS PROGRAM

L.-M. Seillé[1], V. Buat[1,2], V. Fernandez[3] and the CEERs team

Abstract. Stellar emission and hydrogen recombination lines reflect the star formation process at very different timescales and their combination should allow to get the star formation history of galaxies. However dust attenuation hampers any simple comparison because of the variable shape of dust attenuation curves and the differential amount of attenuation of the continuum and line emission. We aim to determine the respective amount of attenuation and the attenuation law at work in the combined ISM and birth clouds inspired by the original Charlot & Fall (2000) recipe. We select 14, $1 < z < 3$ galaxies observed by the CEERS/JWST program and we combine NIRCam photometry with Paschen and Balmer emission lines from NIRSpec. CFHT, HST and Spitzer measurements are added to obtain a multi-wavelength dataset. We will show that we are able to simultaneously fit the spectroscopic and photometric data of these objects using a new method based on equivalent widths (EWs) and we calculate consistent dust attenuation parameters.

Keywords: galaxies, ISM, SED fitting, JWST, EWs

1 Introduction

Hydrogen recombination lines provide critical constraints on the star-formation rates (SFRs) and dust reddening towards the ionised regions of star-forming galaxies. The lines are less extinguished than the far-UV continuum, and can even be measured from the ground with high signal-to-noise (SNR) for individual star-forming objects up to redshift $z \sim 2.6$. Multi-object near-IR spectrographs (e.g., Keck/MOSFIRE, VLT/KMOS) and space-based instruments (e.g., HST/WFC3 grism) provided scientists with hydrogen lines and nebular reddening measurements for a large number of sources up to $z \sim 2.6$ (e.g., Reddy et al. (2020), Battisti et al. (2022)).

On average, the nebular reddening exceeds that of the stellar continuum and these differences are usually attributed to higher dust column densities located around young massive stars which are still embedded in their birth molecular clouds as shown in Charlot & Fall (2000). The recently-launched James Webb Space Telescope (JWST) and its NIRSpec instrument now offer the wavelength coverage and sensitivity to detect Paschen lines. Paschen lines can track the SFR more closely as they are less affected by dust attenuation than the Balmer lines.Combining Paschen and Balmer lines can provide also help on constraining the nebular reddening and the associated characteristics of the ISM.

2 Sample selection

Our sample of 14 galaxies includes measurements over the full NIRCam wavelength range in the F115W, F150W, F200W, F277W, F356W, F410M, and F444W filters, HST/CANDELS ACS_WFC3 F606W and F814W bands, CFHT/Megacam u* and g'. Some objects have additional detections in the far-infrared which are also used when avalaible. To be able to probe the shape of the attenuation curve, Balmer and Paschen lines observed with NIRSpec gratings are necessary as they probe vastly different stellar populations so we require our objects to have at least one Balmer and one Paschen line with an equivalent width (EW) $S/N \geq 5$ (other Balmer and Paschen lines are allowed a $SNR \geq 3$). Finally, we exclude all objects hosting a potential active galactic nucleus (AGN) by checking their [NII]λ658/Hα.

[1] Aix-Marseille Univ, CNRS, CNES, LAM, Marseille, France
[2] Institut Universitaire de France (IUF)
[3] University of Michigan (Schmidt Futures), USA

ID	Redshift	log NII(658)/Hα	Usable line EWs
23542	1.277	-0.78	**Hα, Hβ, Paα, Paβ, Paγ**
5113	1.402	-0.79	**Hα, Paα**
8736	1.553	-0.66	**Hα, Hβ,** Hγ, **Paα,** Paβ
8515	1.567	-0.77	**Hα, Hβ, Hγ, Hδ, Paα, Paβ,** Paγ
5430	1.676	-0.31	**Hα, Hβ, Paβ** , Paγ
10293	1.676	-0.53	**Hα, Hβ, Paα**
6563	1.699	-0.63	**Hα, Hβ, Hγ, Paα, Paβ, Paγ**
5409	1.699	×	**Hα, Hβ, Paα, Paβ**
5300	2.136	×	**Hα, Hβ, Hγ, Hδ, Paβ, Paγ**
3788	2.295	-1.23	**Hα, Hβ, Hγ, Hδ, Paβ, Paγ**
8588	2.336	-0.35	**Hα,** Hβ, Hγ, **Paβ, Paγ**
8710	2.337	-1.05	**Hα, Hβ, Hγ, Paγ**
16991	2.540	-1.28	**Hα,** Hβ, **Hδ,** Paβ, **Paγ**
18294	2.635	×	**Hα, Hβ,** Hγ, **Paβ**

Table 1. Characteristics of the objects used for the study. The spectroscopic redshifts are the mean of the estimated spectroscopic redshift of each line. A cross indicates an absence of [NII]λ(658) detection. Available lines with an EW S/N ≥ 5 are in bold.

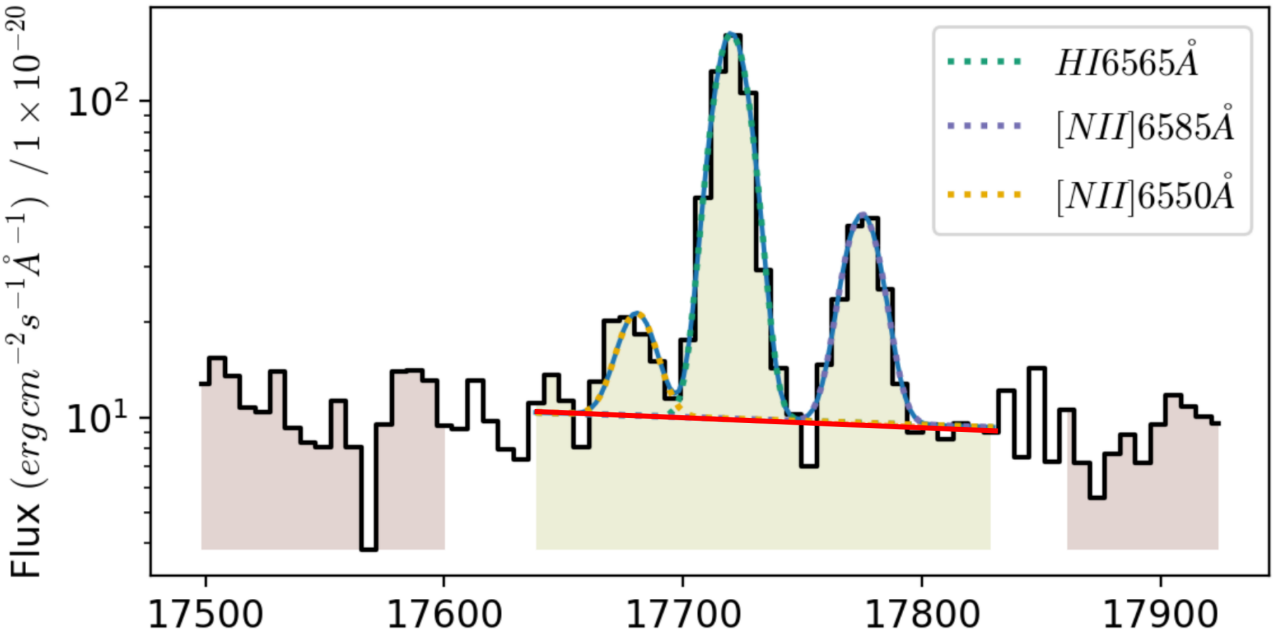

Fig. 1. An example of the new computation method for the [NII] doublet and Hα line. Continua regions are coloured in pink with their linear fit in red while line regions are in green. Note that we can easily deblend all three lines with this computation. Credit to V. Fernandez for the plot.

3 Spectral energy distribution fitting

In this work, we are fitting photometric data and EWs at the same time using the the modelling software CIGALE. We developped a new SED fitting module to reproduce the exact measurements of the EWs made by the CEERs team. The line fluxes are measured using the beta release of LiMe by Fernández et al. (2023). The reported flux uncertainty comes from the standard error definition of the least-squares trust-region method. This uncertainty is propagated to the equivalent width calculation. In this computation, the linear continuum flux and its standard deviation, is derived from two adjacent continua bands. These continua regions are manually adjusted for every line, to guarantee a representative linear continuum measurement and to avoid artefacts (see Fig. 1). With this method, non-symmetrical lines are now accurately modelled and the continuum can be

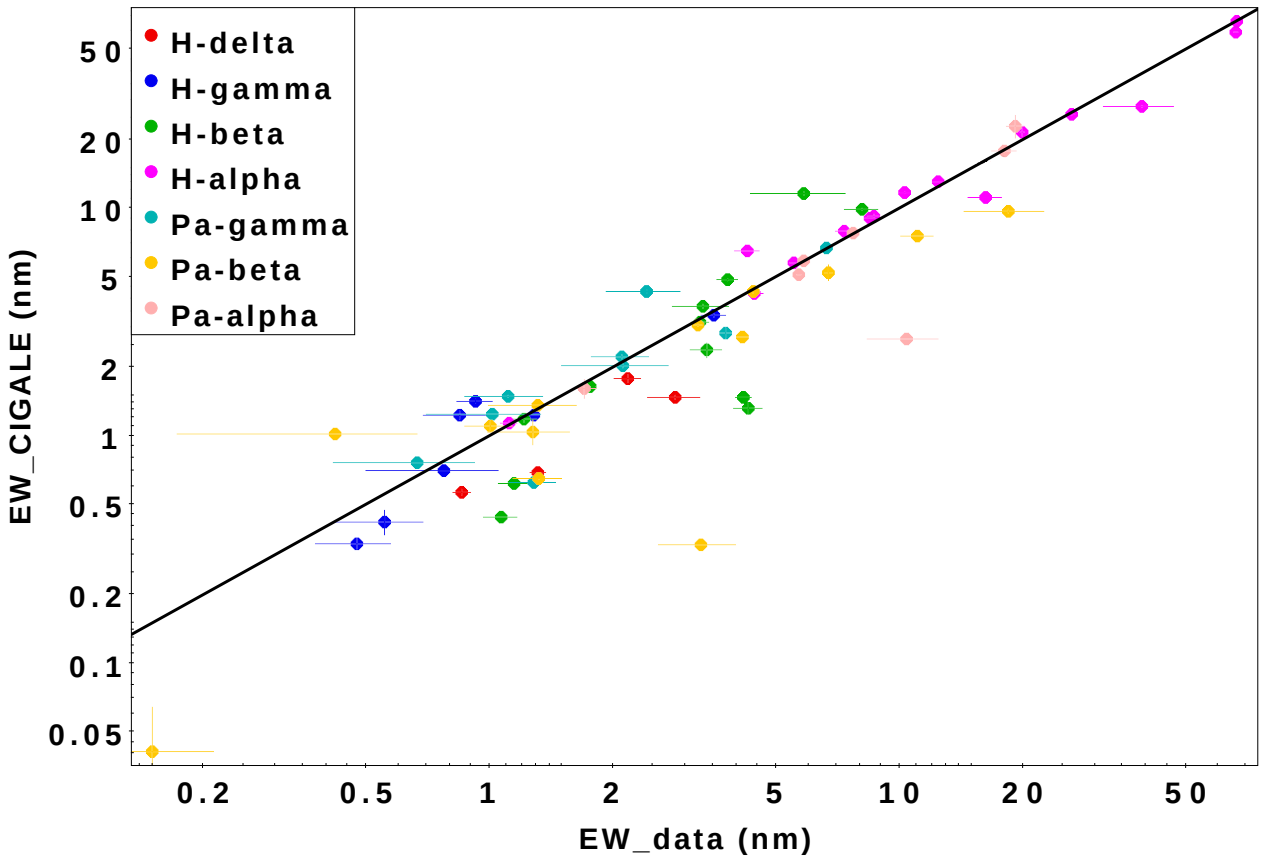

Fig. 2. Result of the fitting of the EWs. Data are on the x-axis while the fit of the EW made by CIGALE is on the y-axis. The black line is the 1:1 relation.

taken anywhere, thus making sure that absorption and other emission lines are avoided. The LiMe fittings for these spectra can be found at the interactive repository at `https://ceers-data.streamlit.app/`, using the corresponding Object ID.

4 Results of SED fitting

As can be seen in Fig. 2, the new method used to fit the EWs in CIGALE is very powerful at reproducing the data of our 14 galaxies. We notice that the fainter a line gets, the more difficult it is to fit it accurately. We can also use CIGALE to get the total attenuation curve of an object from the UV to the near-infrared. We show in Fig. 3 that we are able to reconstruct this curve and different galaxies are exhibiting different dust attenuation parameters. We are seeing a spread in the UV but no extreme values for the power law exponent. However, there is a clear separation between steep and flat curves in the IR part of the spectrum.

5 Conclusions

We are studying 14 objects between 1 < z < 3 observed by JWST to probe the shape of the total attenuation curve. To do this, we implemented a new EWs fitting method in CIGALE to reproduce exactly the line measurements and computations done by the CEERs team. With this method, we obtain an overall very good agreement between the fits and the data. We are able to reconstruct the total attenuation curve of every object in our sample and also to get the differential amount of attenuation between young and old stars. However, we still need to address the possible attenuation parameters degeneracy.

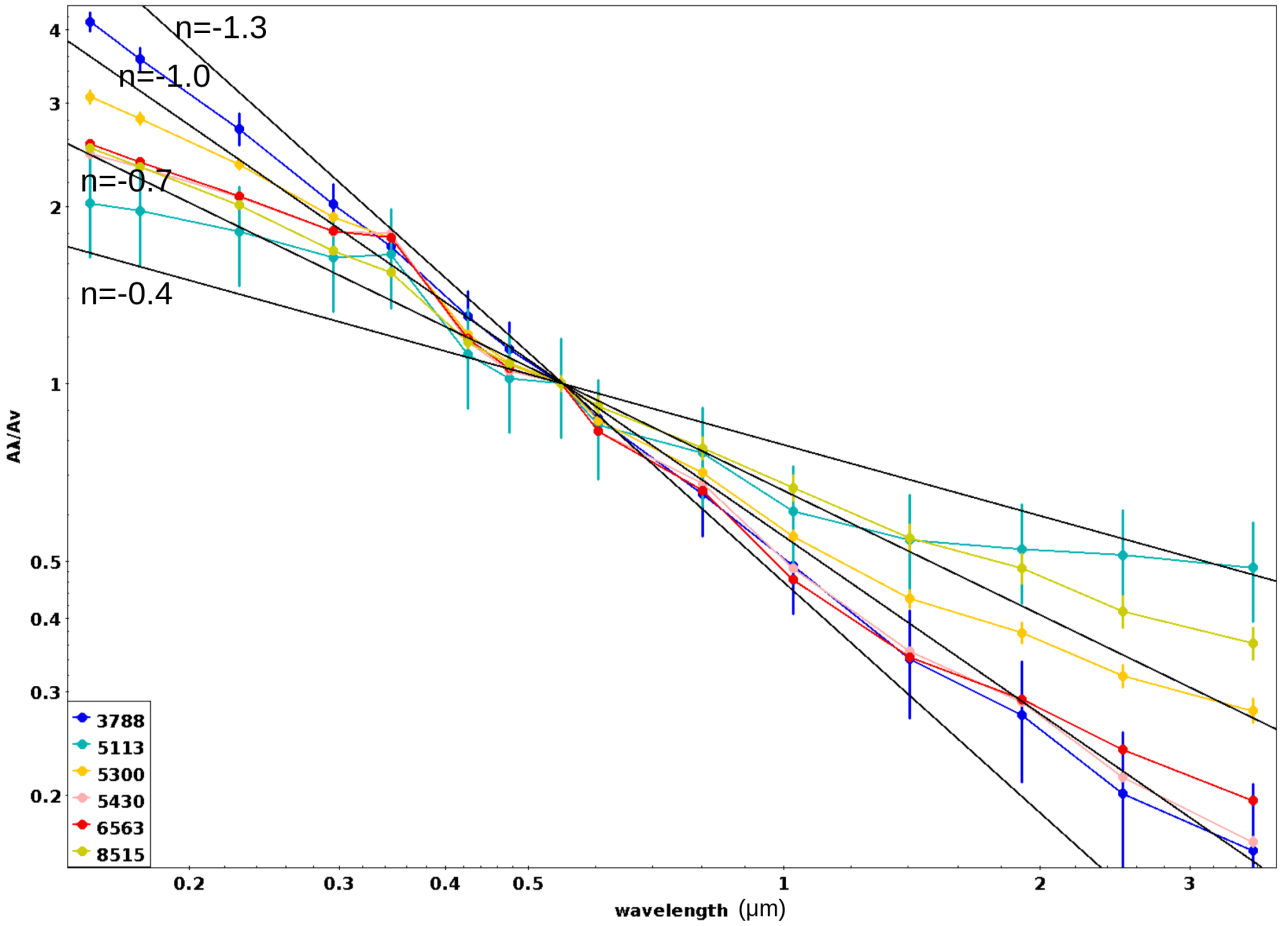

Fig. 3. Examples of total attenuation curves from objects in our sample compared to power laws with varying exponents in black.

References

Battisti, A. J., Bagley, M. B., Baronchelli, I., et al. 2022, MNRAS, 513, 4431
Charlot, S. & Fall, S. M. 2000, ApJ, 539, 718
Fernández, V., Amorín, R., Sanchez-Janssen, R., del Valle-Espinosa, M. G., & Papaderos, P. 2023, MNRAS, 520, 3576
Reddy, N. A., Shapley, A. E., Kriek, M., et al. 2020, ApJ, 902, 123